DNS OF PASSIVE SCALAR TRANSPORT IN TURBULENT SUPERSONIC CHANNEL FLOW

Holger Foysi, Rainer Friedrich
Fachgebiet Strömungsmechanik
TU München, Boltzmannstr. 15, D-85748 Garching, Germany
holger@flm.mw.tu-muenchen.de, r.friedrich@flm.mw.tu-muenchen.de

ABSTRACT

Direct numerical simulations of compressible turbulent channel flow with passive scalar transport are performed at three Reynolds numbers Re_τ ranging from 221 to 545 and Mach numbers ranging from 1.5 to 3.0. The Prandtl and Schmidt numbers are 0.7 and 1.0, respectively. A mean scalar gradient is imposed across the mean flow. Budgets of the scalar variance and the scalar flux components are presented for these flow parameters and Mach number effects are discussed. Outer scalings are found suitable to collapse incompressible and compressible data.

INTRODUCTION

Incompressible fully developed turbulent channel flow with passive scalar transport has been directly simulated for the first time by Kim *et al.* (1989) at a Reynolds number Re_τ, based on the friction velocity, u_τ, and the channel half width, h of 180. Two types of boundary conditions were used, in the first case the scalar was internally generated with isothermal walls of the same temperature, in the second case a different scalar magnitude on each of the isothermal walls was imposed. The Prandtl numbers were varied between 0.1 and 2. Recently Johansson *et al.* (1999) performed a similar DNS, imposing a mean scalar gradient, at a Reynolds number of $Re_\tau = 265$. Not much is known so far about the influence of compressibility on the transport of a passive scalar although its thorough understanding is prerequisite to the understanding of active scalar transport and combustion processes. Investigations of compressibility effects in supersonic channel flow have been presented first by Coleman *et al.* (1995), by Huang *et al.* (1995) and later by Lechner *et al.* (2001). They all used isothermal walls, a domain size of $(L_x,L_y,L_z) = (4\pi,4\pi/3,2)$h in streamwise, spanwise and wall normal direction and Mach numbers between 1.5 (Coleman,1995, Huang, 1995, Lechner, 2001) and 3 (Coleman,1995, Huang, 1995). Coleman *et al.* (1995) and Huang *et al.* (1995) demonstrated that a van Driest transformation of the mean velocity and a semi-local near-wall scaling for r.m.s. velocity and vorticity fluctuations collapse compressible and incompressible data onto practically the same curves. Foysi, Sarkar and Friedrich (these Proceedings) give further details concerning compressibility effects on Reynolds stresses and the pressure-rate-of-strain tensor. This paper addresses the response of the turbulent scalar fluxes and scalar variance to Mach and Reynolds number variations in fully developed compressible channel flow. Budgets of the scalar variance and streamwise as well as wall-normal scalar fluxes are shown and discussed.

NUMERICAL METHOD AND COMPUTATIONAL DETAILS

The compressible Navier-Stokes equations are solved in a pressure-, velocity-, entropy-form (Sesterhenn, 2001). These equations are supplemented by a transport equation for the passive scalar. In Cartesian coordinates the whole set of equations reads:

$$\frac{\partial p}{\partial t} = -u_j\frac{\partial p}{\partial x_j} - \gamma p\frac{\partial u_j}{\partial x_j} + (\gamma-1)\left(\Phi - \frac{\partial q_j}{\partial x_j}\right), \quad (1)$$

$$\frac{\partial u_i}{\partial t} = -u_j\frac{\partial u_i}{\partial x_j} - \frac{1}{\rho}\left(\frac{\partial p}{\partial x_i} - \frac{\partial \tau_{ij}}{\partial x_j}\right) + \frac{1}{\rho}f_1\delta_{i1}, \quad (2)$$

$$\frac{\partial s}{\partial t} = -u_j\frac{\partial s}{\partial x_j} + \frac{R}{p}\left(\Phi - \frac{\partial q_j}{\partial x_j}\right), \quad (3)$$

$$\frac{\partial \xi}{\partial t} = -u_j\frac{\partial \xi}{\partial x_j} + \frac{1}{\rho}\frac{\partial}{\partial x_j}\left(\rho D\frac{\partial \xi}{\partial x_j}\right), \quad (4)$$

where p, u_i, s, ρ, ξ represent pressure, Cartesian velocity components, entropy, density and concentration, respectively. The components of the heat flux vector $\mathbf{q}$, viscous stress tensor τ and the dissipation rate Φ read:

$$q_i = -\lambda\frac{\partial T}{\partial x_i}, \quad \tau_{ij} = 2\mu s_{ij} - \frac{2}{3}\mu s_{kk}\delta_{ij}, \quad (5)$$

$$\Phi = \tau_{ij}s_{ij}, \quad s_{ij} = \frac{1}{2}\left(\frac{\partial u_i}{\partial x_j} + \frac{\partial u_j}{\partial x_i}\right). \quad (6)$$

The thermal equation of state

$$p = \rho RT, \quad R = C_p - C_v, \quad (7)$$

and the following laws for dynamic viscosity μ, heat conductivity λ and diffusivity D close the set of equations:

$$\frac{\mu}{\mu_{ref}} = \left(\frac{T}{T_{ref}}\right)^n, \quad \lambda = \mu\frac{C_p}{Pr}, \quad D = \frac{\mu}{\rho Sc}, \quad n = 0.7 \quad (8)$$

The Prandtl number Pr, the Schmidt number Sc and the ratio of specific heats γ are kept at constant values in the temperature and concentration ranges considered, namely $Pr = 0.7$, $Sc = 1.0$, $\gamma = C_p/C_v = 1.4$. The body force term $f_1\delta_{i1}$ in the momentum equation replaces the mean pressure gradient in streamwise direction and is uniform in 3D space. Thus, fully developed turbulent flow can be handled using periodic boundary conditions in stream- and spanwise directions. A mean scalar gradient is imposed on the flow, using an initial profile of the form (Johansson, 1999)

$$\xi(x_1,x_2,x_3,0) = \log_{10}\left\{\frac{z_0+x_3}{z_0-x_3}\right\}/\log_{10}\left\{\frac{z_0+1}{z_0-1}\right\}, \quad z_0 = 1.007 \quad (9)$$

and the bondary conditions $\xi(x_1,x_2,0,t) = 1$, $\xi(x_1,x_2,2,t) = -1$. This corresponds to an injection of the scalar from one wall and a removal from the other.

Following Sesterhenn (2001) equations (4) are cast in a characteristic non-conservative form, compare Foysi *et al.* (2003) in these Proceedings, which allows to formulate wall boundary conditions consistently with the field equations.

A compact 5th-order upwind scheme of Adams and Shariff (1996) is used to discretize the hyperbolic (Euler) terms in the basic equations. The molecular transport terms are discretized with a compact 6th order scheme of Lele (1992). The solution is advanced in

Table 1: Flow and computational parameters

Case	M	Re	Re_τ	L_{x_1}/h	L_{x_2}/h	L_{x_3}/h
A	1.5	3000	221	4π	$4\pi/3$	2
B	2.5	5000	455	2π	$2\pi/3$	2
C	3.0	6000	545	2π	$2\pi/3$	2

Table 2: Flow and computational parameters (cont.)

Case	N_{x1}	N_{x2}	N_{x3}	Δx_1^+	Δx_2^+	$\Delta x_{3\,\max}^+$
A	192	128	151	14.46	7.23	5.02
B	256	128	201	11.16	7.44	7.46
C	256	128	201	13.37	8.91	9.38

time with a third-order 'low-storage' Runge-Kutta scheme, proposed by Williamson (1980). Three direct simulations have been performed for different *flow parameters*. The global Mach and Reynolds numbers for fully developed channel flow read

$$M = u_{av}/c_w, \quad Re = \rho_m u_{av} h/\mu_w. \tag{10}$$

The bulk-averaged density ρ_m is defined as $\rho_m = \int_0^h \overline{\rho} dx_3/h$, u_{av} is the Reynolds (rather than Favre) cross-sectionally averaged velocity. The speed of sound and viscosity are computed for constant wall temperature T_w, while h is the channel half width. The friction Reynolds number $Re_\tau = \rho_w u_\tau h/\mu_w$, with $u_\tau = \sqrt{\tau_w/\rho_w}$, is a result of the simulation. Tables 1 and 2 summarize the flow parameters, box sizes and numbers of grid points used in the three cases A-C. Equidistant grids are used in (x_1,x_2)-directions. In the wall-normal x_3-direction, points are clustered following tanh-functions (Lechner, 2001). The first gridpoint is below $x_3^+ = 1.5$ and the tenth at $x_3^+ \leq 17.62$ (case C).

MEAN FLOW VARIABLES AND TURBULENT TRANSPORT

For fully developed channel flow the integrated mean momentum and scalar transport equations read in wall (+) units:

$$\frac{\bar{\mu}}{\mu_w}\frac{d\tilde{u}_1^+}{dx_3^+} - \frac{\overline{\rho u_1'' u_3''}}{\tau_w} = 1 - \frac{x_3}{h}, \tag{11}$$

$$-\frac{1}{Sc}\frac{\bar{\mu}}{\mu_w}\frac{d\tilde{\xi}^+}{dx_3^+} - \frac{\overline{\rho u_3'' \xi''}}{\chi_w} = 1 \tag{12}$$

In (11,12), a Reynolds averaged velocity and concentration, $\tilde{u}_1, \tilde{\xi}$ have been used to express the mean viscous stress and the mean diffusion flux, while correlations involving viscosity and diffusivity fluctuations have been neglected. On the other hand, it is convenient to use Favre fluctuations in defining Reynolds stresses, $\overline{\rho u_i'' u_j''}$, and turbulent scalar fluxes, $\overline{\rho \xi'' u_j''}$. Wall units with respect to the momentum transport are the friction velocity $u_\tau = \sqrt{\tau_w/\rho_w}$, as well as density and viscosity at the wall, ρ_w, μ_w. With respect to the scalar transport these are u_τ, ρ_w, μ_w and the friction scalar ξ_τ, resulting from the scalar wall flux χ_w:

$$\chi_w = \left.\overline{\frac{\mu}{Sc}\frac{\partial \xi}{\partial x_3}}\right|_w = -\rho_w u_\tau \xi_\tau. \tag{13}$$

From (12) we conclude that the sum of molecular and turbulent scalar fluxes is constant across the channel, much like the total shear stress is a constant in turbulent Couette flow. The molecular scalar flux is non-zero in the channel core, due to an S-shaped profile of the mean scalar with non-zero gradient at the centreline. Figure 1 shows profiles of the Favre-averaged scalar, $\tilde{\xi}$, normalized by wall values, for cases A-C and incompressible flow at $Re_\tau = 265$, $Sc = 0.7$, according to Johansson *et al.* (2001). In order to see the effect of Mach number on the molecular scalar flux, we plot its exact value $\overline{\mu/Sc \partial\xi/\partial x_3}$ normalized with $|\chi_w|$ in Figure 2. In the core region all three cases practically collapse onto one curve. Effects of Mach number appear where mean density and viscosity have their strongest variations.

Outer scaling: From (12) and the fact that the molecular scalar flux is small (Figure 2) compared to its turbulent counterpart, we assume that $|\chi_w|$ is a reasonable outer scale of the turbulent scalar flux in wall-normal direction. Figures 3 and 4 demonstrate that this is true in the range of $x_3/h > 0.6$ for the streamwise scalar flux as well, irrespective of the Mach and Reynolds number. Incompressible data of Johansson *et al.* (2001) for $Sc = 0.71$ are included in the Figures for comparison.

Inner scaling: From (11,12), neglecting turbulent fluxes near the wall, we get for the viscous sublayer:

$$-\frac{d\tilde{\xi}^+}{dx_3^+} = \frac{\mu_w}{\bar{\mu}} Sc, \quad \frac{d\tilde{u}_1^+}{dx_3^+} = \frac{\mu_w}{\bar{\mu}}, \tag{14}$$

and after integration

$$\tilde{\xi}_w^+ - \tilde{\xi}^+ = Sc\,\tilde{u}_1^+ \tag{15}$$

Equation (14) suggests the following transformed velocity and scalar in the viscous sublayer:

$$\tilde{u}_{1,v}^+ := \int_0^{\tilde{u}_1^+} \frac{\bar{\mu}}{\mu_w} d\tilde{u}_1^+ = x_3^+ = -\frac{1}{Sc}\int_{\tilde{\xi}_w^+}^{\tilde{\xi}^+} \frac{\bar{\mu}}{\mu_w} d\tilde{\xi}^+ =: \tilde{\xi}_v^+ \tag{16}$$

Figure 5 contains profiles of the viscosity transformed scalar $\tilde{\xi}_v$, according to equation (16), together with x_3^+. The graph shows that the different cases deviate only beyond the buffer layer.

BUDGETS OF THE SCALAR VARIANCE AND SCALAR FLUXES

For steady and fully developed compressible channel flow the transport equation for the scalar variance, $\overline{\rho\xi''^2}/2$, reads:

$$0 = -\overline{\rho u_3'' \xi''}\frac{\partial \tilde{\xi}}{\partial x_3} - \frac{\partial}{\partial x_3}\overline{\rho u_3'' \xi''^2}/2 + \frac{\partial}{\partial x_3}\left(\overline{\frac{\mu}{Sc}\frac{\partial \xi''^2/2}{\partial x_3}} + \overline{\frac{\mu}{Sc}\xi''\frac{\partial \xi''}{\partial x_3}}\right) - \overline{\frac{\mu}{Sc}\frac{\partial \xi''}{\partial x_3}\frac{\partial \xi''}{\partial x_3}} - \overline{\frac{\mu}{Sc}\frac{\partial \xi''}{\partial x_j}\frac{\partial \xi''}{\partial x_j}} \tag{17}$$

The terms on the r.h.s. represent production by mean scalar gradients, turbulent transport and viscous diffusion and dissipation. A production term due to mean dilatation does not exist in this flow. At the wall viscous diffusion and dissipation balance.

The transport equations for the turbulent streamwise and wall-normal scalar fluxes, $\overline{\rho u_1'' \xi}$ and $\overline{\rho u_3'' \xi}$ are, respectively:

$$\begin{aligned} 0 = {} & -\overline{\rho u_1'' u_3''}\frac{\partial \tilde{\xi}}{\partial x_3} - \overline{\rho \xi'' u_3''}\frac{\partial \tilde{u}_1}{\partial x_3} - \frac{\partial}{\partial x_3}\overline{\rho u_1'' u_3'' \xi''} - \overline{\xi''\frac{\partial p}{\partial x_1}} \\ & + \frac{\partial}{\partial x_3}\left(\overline{u_1''\frac{\mu}{Sc}\frac{\partial \xi}{\partial x_3}} + \overline{\xi''\tau_{13}}\right) - \overline{\tau_{1j}\frac{\partial \xi''}{\partial x_j}} - \overline{\frac{\mu}{Sc}\frac{\partial \xi}{\partial x_j}\frac{\partial u_1''}{\partial x_j}} \end{aligned} \tag{18}$$

$$\begin{aligned} 0 = {} & -\overline{\rho u_3''^2}\frac{\partial \tilde{\xi}}{\partial x_3} - \frac{\partial}{\partial x_3}\overline{\rho u_3''^2 \xi''} - \overline{\xi''\frac{\partial p}{\partial x_3}} \\ & + \frac{\partial}{\partial x_3}\left(\overline{u_3''\frac{\mu}{Sc}\frac{\partial \xi}{\partial x_3}} + \overline{\xi''\tau_{33}}\right) - \overline{\tau_{3j}\frac{\partial \xi''}{\partial x_j}} - \overline{\frac{\mu}{Sc}\frac{\partial \xi}{\partial x_j}\frac{\partial u_3''}{\partial x_j}} \end{aligned} \tag{19}$$

Both transport equations contain production terms due to mean scalar gradients, the streamwise scalar flux is in addition produced by mean velocity gradients. The other terms denote the turbulent transport of the scalar fluxes, a scalar-pressure-gradient correlation, the analogue of the velocity-pressure-gradient term in the Reynolds stress transport equation and, finally, the transport of both scalar fluxes by two molecular diffusion terms and two destruction terms (viscous and diffusive destruction).

Scalar variance: For convenience, we first show profiles of the r.m.s. scalar fluctuations, normalized by $\tilde{\xi}_{av} = \int_0^1 \tilde{\xi} dx_3/h$ in Figure 6. They reveal a peak in the wall layer and a maximum at the channel centreline which is due to non-zero gradients of the mean scalar there, resulting in higher peaks for the lower Mach and Reynolds number cases A,B, which have steeper gradients. Incompressible data of Johansson *et al.* (2001) are plotted for comparison. They match the present $M = 3$ data. The increase in wall peaks, compared to incompressible flow, is in line with the corresponding increase in the streamwise Reynolds stress as Ma increases (see Figure 7) and the increase in the streamwise scalar flux, $\overline{\rho u_1'' \xi''}$ in Figure 4. These effects underline the strong similarity of the u_1'' and ξ'' fields at high Mach numbers. For annular mixing layers this effect has been explained by Freund *et al.* (1997) based on the transport equations for ρu_1 and $\rho\xi$ and the suppressed role of the pressure. In the wall layer of the channel the behaviour of the pressure is similar, but may be due to other reasons which are currently explored.

Figure 8 shows profiles of four terms in the scalar variance budget normalized by $\xi_{av}|\chi_w|/h$ for case C alone. In the channel core, production and dissipation of scalar fluctuations balance and are non-zero due to a finite scalar gradient. In the buffer layer where most of the turbulent kinetic energy is produced, all terms contribute to the budget. At the wall itself, dissipation and molecular diffusion balance. In order to show effects of Mach number, we have plotted production and dissipation profiles separately, for cases A-C and the incompressible data of Johansson *et al.*(2001). In the core region, incompressible and compressible producion rates collapse (Figure 9), indicating that $\xi_{av}|\chi_w|/h$ is the proper outer scale. In the wall layer we notice an increase as the Reynolds number increases. The peak prodution rate can be computed using the extremum condition, expressed in wall units:

$$d\left(\frac{-\overline{\rho u_3'' \xi''}}{\chi_w}\frac{\partial \tilde{\xi}^+}{\partial x_3^+}\right)/dx_3^+ = 0 \qquad (20)$$

We make the approximation $\bar{\xi} \simeq \tilde{\xi}$ and substitute the scalar flux from equation (12) into (20) to get:

$$-\frac{1}{Sc}\frac{\bar{\mu}}{\mu_w}\frac{d\tilde{\xi}^+}{dx_3^+} = \frac{1}{2}\left(1 + \frac{1}{Sc}\frac{d\bar{\mu}/\mu_w}{dx_3^+}\left(\frac{d\tilde{\xi}^+}{dx_3^+}\right)^2 / \frac{d^2\tilde{\xi}^+}{dx_3^{+2}}\right). \qquad (21)$$

From this relation we conclude that the molecular scalar flux is increased due to viscous heating in compressible flow compared to incompressible flow ($\bar{\mu}/\mu_w = 1$). Since the term in the brackets is greater than one, we get

$$-\frac{1}{Sc}\frac{\bar{\mu}}{\mu_w}\frac{d\tilde{\xi}^+}{dx_3^+} > \frac{1}{2} \qquad (22)$$

while in incompressible flow

$$-\frac{1}{Sc}\frac{d\tilde{\xi}^+}{dx_3^+} = \frac{1}{2}. \qquad (23)$$

For the peak production rate of the scalar variance we therefore get (using (12), (22))

$$-\frac{\overline{\rho u_3'' \xi''}}{\chi_w}\frac{d\tilde{\xi}^+}{dx_3^+} < \frac{1}{4}Sc. \qquad (24)$$

In incompressible flow the non-dimensional production rate has a peak value of $Sc/4$. Hence, the scalar variance production rate in the compressible wall layer is reduced in a way similar to the reduction of turbulent kinetic energy production. Note that the data of Johansson *et al.* (2001) are obtained for a Schmidt number of 0.7 which (for the same Reynolds number) reduces the peak production rate. This is brought out in Figure 10 where all production terms are normalized by χ_w^2/μ_w. Profiles of the scalar variance dissipation rate are plotted in Figure 11 using the same normalization. It is seen that the Mach number effect reduces the scalar dissipation rate everywhere in the channel. A similar effect has been observed for the turbulent kinetic energy dissipation rate. Comparison with Johansson *et al.*'s (2001) data reveals a Schmidt number effect as well.

Budget of streamwise flux: The budget for Case C is presented in Figure 12, normalized by $|\chi_w|\tau_w/\mu_w$. It has the interesting feature that all terms vanish at the channel centreline. In the core region, production and the scalar-pressure-gradient correlation dominate, while the destruction rate is comparably small. Only at the wall exists a balance between destruction and molecular diffusion terms. It turns out that $u_{av}|\chi_w|/h$ is the proper outer scale for the $\overline{\rho u_1'' \xi''}$ -production, see Figure 13 (this can be seen, too, by integrating the streamwise scalar-flux balance from the wall to the channel core and estimating the remaining non-zero terms), while wall scaling ($\tau_w|\chi_w|/\mu_w$) reveals the Mach number effect in terms of a reduction of the peak production rate with increasing Mach number. The scalar-pressure-gradient correlation, $\overline{\xi'' \partial p/\partial x_1}$, in Figure 14 scales as $u_{av}|\chi_w|/h$ in the channel core for compressible and incompressible flow.

Budget of wall-normal flux: Unlike the case of streamwise flux, none of the terms vanishes on the centreline. In Figure 15, representing case C, we note the dominance of production and scalar-pressure-gradient correlation, $\overline{\xi'' \partial p/\partial x_3}$. At the wall destruction and diffusion balance, but have so small values that they cannot be distinguished on the plot. Again, $u_{av}|\chi_w|/h$ turns out to be the proper outer scale for the scalar flux production and the scalar-pressure gradient correlation. Figures 16 and 17 show the Mach number effect for these terms, namely reduced production and reduced scalar-pressure-gradient correlation as the Mach number increases. The Reynolds number effect is less pronounced.

CONCLUSIONS

Passive scalar transport in compressible turbulent channel flow reveals features similar to turbulent momentum transport, namely

- an increase of the scalar flux peak values with increasing Reynolds number
- a decrease of the wall-normal scalar flux and an increase of the streamwise scalar flux magnitude due to compressibility.

These effects are in line with the behaviour of the corresponding Reynolds stresses. Similar to the production of the Reynolds stresses and the TKE are the production rates of the scalar variance and the scalar fluxes reduced when the flow becomes compressible. The peak production of $\overline{\rho \xi''^2}/2$ is $< Sc/4$ when normalized by wall units. The scalar-pressure-gradient correlations scale as $u_{av}|\chi_w|/h$ in the channel core and show reduced amplitudes in the compressible wall layer, most probably due to the suppressed role of the pressure fluctuations there.

REFERENCES

N.A. Adams, K. Shariff: "A high-resolution hybrid compact-ENO scheme for shock-turbulence interaction problems". JCP **127**, 1996, pp. 27

G.N. Coleman, J. Kim, R.D. Moser: "Turbulent supersonic isothermal-wall channel flow". J. Fluid Mech. **305**, 1995, pp. 159-183

P.G. Huang, G.N. Coleman, P. Bradshaw: "Compressible turbulent channel flows: DNS results and modelling". J. Fluid Mech. **305**, 1995, pp. 185-218

A.V. Johansson, P.M. Wikström: "DNS and Modelling of Passive Scalar Transport in Turbulent Channel Flow with Focus on Scalar Dissipation Rate Modelling". Flow, Turb. and Combustion **63**, 1999, pp. 223-245

H. Foysi, S. Sarkar, R. Friedrich: "On Reynolds stress anisotropy in compressible channel flow." Proc. of the 3rd TSFP Conference, Sendai, Japan, 2003.

J.B. Freund, P.Moin, S.K. Lele: "Compressibility effects in a turbulent annular mixing layer." Dept. of Mech. Eng., Stanford Univ. Report No. TF-72, 1997.

J. Kim, P. Moin, R.D. Moser:"Turbulence statistics in fully developed channel flow at low Reynolds number". J. Fluid Mech. **177**, 1987, pp. 133

J. Kim, P. Moin: "Transport of passive scalars in a turbulent channel flow." Turbulent Shear flows 6, Springer-Verlag, Berlin (1989), pp. 85-96.

R. Lechner, J. Sesterhenn, R. Friedrich: "Turbulent supersonic channel flow". J. Turbulence **2**, 2001, pp. 1-25

S. Lele: "Compact Finite Difference Schemes with Spectral-like Resolution". J. Comp. Phys. **103**, 1992, pp. 16-42

Y. Morinishi, S. Tamano, K. Nakabayashi: "A DNS algorithm using B-spline collocation method for compressible turbulent channel flow". Computers & Fluids **32**, 2003, pp. 751-776

R.D. Moser, J. Kim, N.N. Mansour: "Direct numerical simulation of turbulent channel flow up to $Re_\tau = 590$". Phys. Fluids **11**, 1999, pp. 943-945

J. Sesterhenn: "A characteristic-type formulation of the Navier–Stokes equations for high order upwind schemes". Computers & Fluids **30**, 2001, pp. 37

J.H. Williamson: "Low-storage Runge-Kutta schemes", J. Comp. Physics **35**, 1980, pp. 48-56

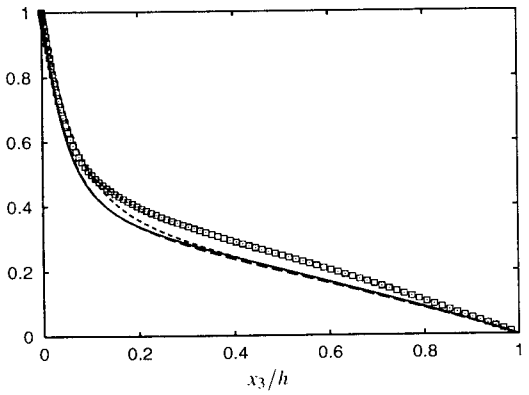

Figure 1: Profiles of $\tilde{\xi}$ normalized by ξ_w. Compressible cases: ——, $Re_\tau = 545$, $Ma = 3$; – – –, $Re_\tau = 455$, $Ma = 2.5$;- - - -, $Re_\tau = 221$, $Ma = 1.5$. □ shows data of Johansson *et al.*, $Re_\tau = 265$; Sc = 0.7

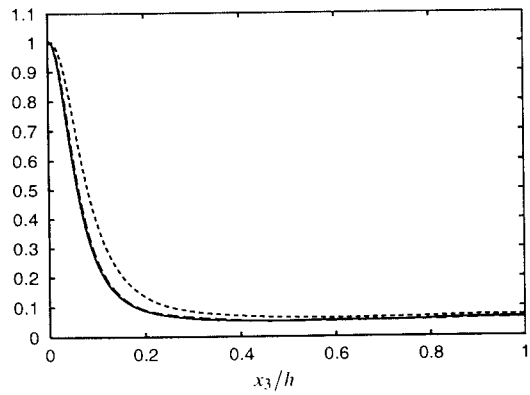

Figure 2: Profiles of $-\overline{\frac{\mu}{Sc}\frac{\partial\tilde{\xi}}{\partial x_3}}$ normalized by $|\chi_w|$. ——, $Re_\tau = 545$, $Ma = 3$; – – –, $Re_\tau = 455$, $Ma = 2.5$;- - - -, $Re_\tau = 221$, $Ma = 1.5$.

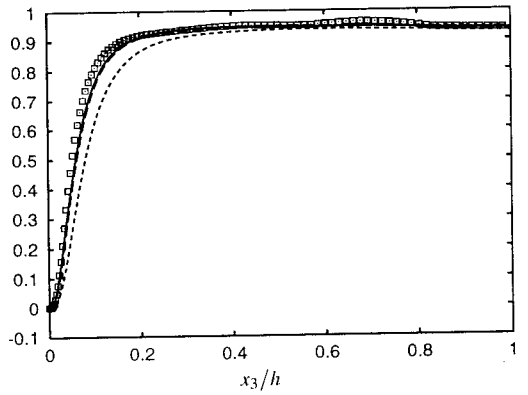

Figure 3: Profiles of the wall normal scalar flux $\overline{\rho u_3'' \xi''}$ normalized by $|\chi_w|$. The compressible cases are: ——, $Re_\tau = 545$, $Ma = 3$; – – –, $Re_\tau = 455$, $Ma = 2.5$;- - - -, $Re_\tau = 221$, $Ma = 1.5$. □ shows data of Johansson *et al.*, $Re_\tau = 265$; Sc = 0.7

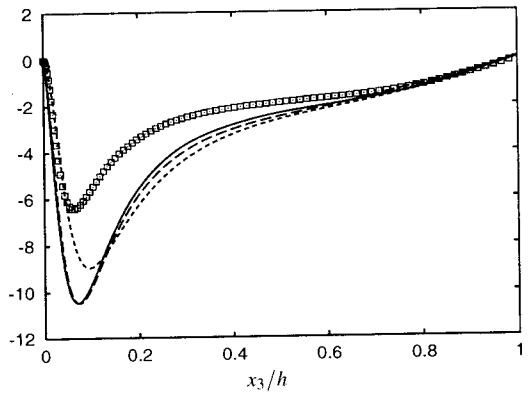

Figure 4: Profiles of the streamwise scalar flux $-\overline{\rho u_1'' \xi''}$ normalized by $|\chi_w|$. The compressible cases are: ——, $Re_\tau = 545$, $Ma = 3$; – – –, $Re_\tau = 455$, $Ma = 2.5$;- - - -, $Re_\tau = 221$, $Ma = 1.5$. □ shows data of Johansson *et al.*, $Re_\tau = 265$; Sc = 0.7

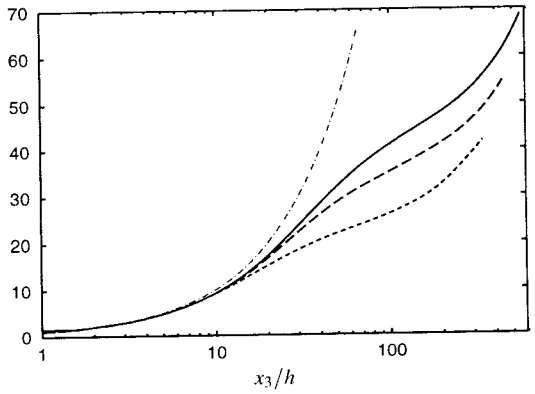

Figure 5: $\tilde{\xi}_v = \int_0^{\tilde{\xi}^+} \tilde{\mu}/\mu_w d\tilde{\xi}^+$. ——, $Re_\tau = 545$, $Ma = 3$; – – –, $Re_\tau = 455$, $Ma = 2.5$;- - - -, $Re_\tau = 221$, $Ma = 1.5$; –·–·–, x_3^+. □ Van Driest transformed scalar, $Re_\tau = 545$, $Ma = 3$

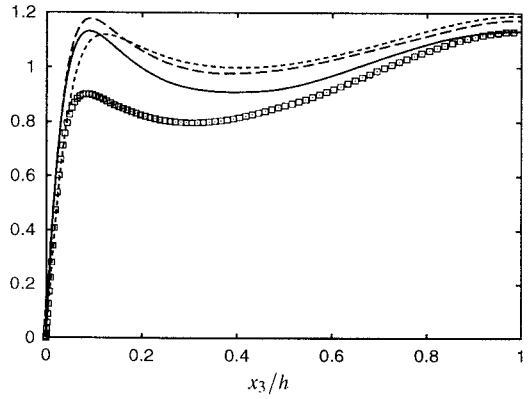

Figure 6: Profiles of the r.m.s. scalar fluctuations $\sqrt{\overline{\xi''^2}}$ normalized by ξ_{av}. Compressible cases: ——, $Re_\tau = 545$, $Ma = 3$; – – –, $Re_\tau = 455$, $Ma = 2.5$;- - - -, $Re_\tau = 221$, $Ma = 1.5$. □ shows data of Johansson *et al.*, $Re_\tau = 265$; Sc = 0.7

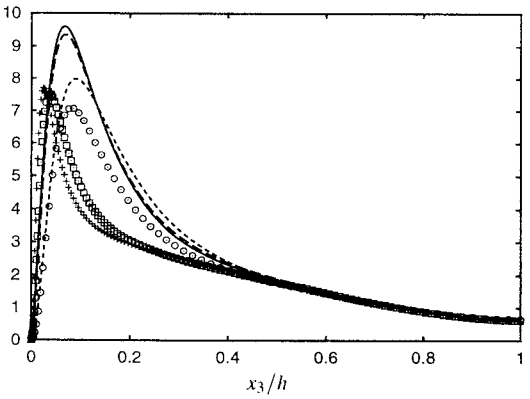

Figure 7: $\overline{\rho u_1''^2}$ normalized by τ_w. *Compressible cases*: ——, $Re_\tau = 545$, $Ma = 3$; – – –, $Re_\tau = 455$, $Ma = 2.5$; - - - -, $Re_\tau = 221$, $Ma = 1.5$. *Incompressible cases* (Moser, 1999): ⊙ $Re_\tau = 180$; □ $Re_\tau = 395$; + $Re_\tau = 590$.

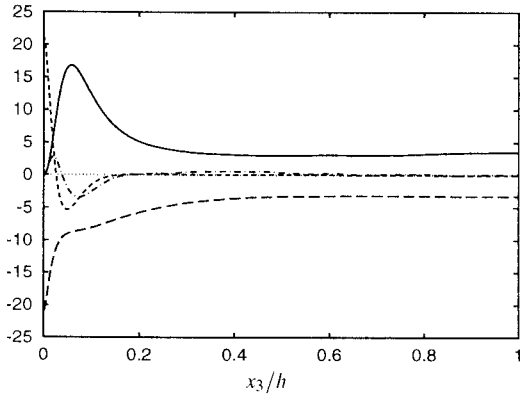

Figure 8: Balance of $\overline{\rho\xi''^2/2}$ for $Re_\tau = 545$, $Ma = 3$, normalized by $\xi_{av}|\chi_w|/h$. ——, $-\overline{\rho u_3''\xi''}\frac{\partial\tilde{\xi}}{\partial x_3}$; – – –, $-\overline{\frac{\mu}{Sc}\frac{\partial\xi''}{\partial x_j}\frac{\partial\xi''}{\partial x_j}} - \overline{\frac{\mu}{Sc}\frac{\partial\xi''}{\partial x_3}\frac{\partial\xi}{\partial x_3}}$; - - - -, $\frac{\partial}{\partial x_3}\left(\overline{\frac{\mu}{Sc}\frac{\partial\xi''^2/2}{\partial x_3}} + \overline{\frac{\mu}{Sc}\xi''\frac{\partial\xi}{\partial x_3}}\right)$; -·-·-, $-\frac{\partial}{\partial x_3}\overline{\rho u_3''\xi''^2/2}$;

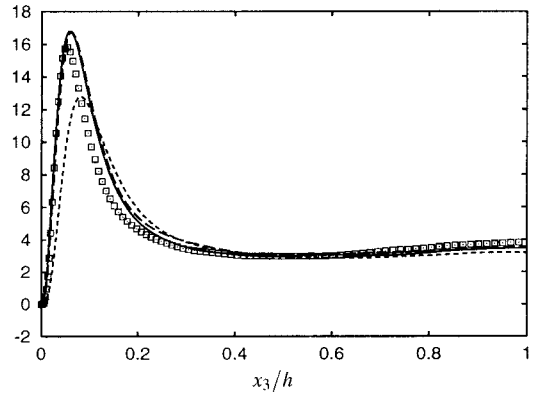

Figure 9: Production term of the $\overline{\rho\xi''^2/2}$-balance, normalized by $\xi_{av}|\chi_w|/h$. ——, $Re_\tau = 545$, $Ma = 3$; – – –, $Re_\tau = 455$, $Ma = 2.5$;- - - -, $Re_\tau = 221$, $Ma = 1.5$. □ shows data of Johansson *et al.*, $Re_\tau = 265$; Sc = 0.7

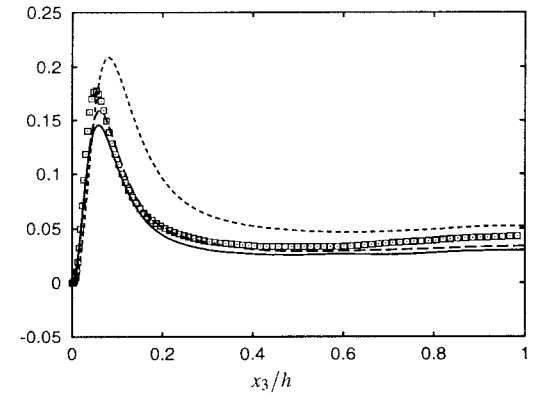

Figure 10: Production term of the $\overline{\rho\xi''^2/2}$-balance normalized by χ_w^2/μ_w. ——, $Re_\tau = 545$, $Ma = 3$; – – –, $Re_\tau = 455$, $Ma = 2.5$;- - - -, $Re_\tau = 221$, $Ma = 1.5$. □ shows data of Johansson *et al.*, $Re_\tau = 265$; Sc = 0.7

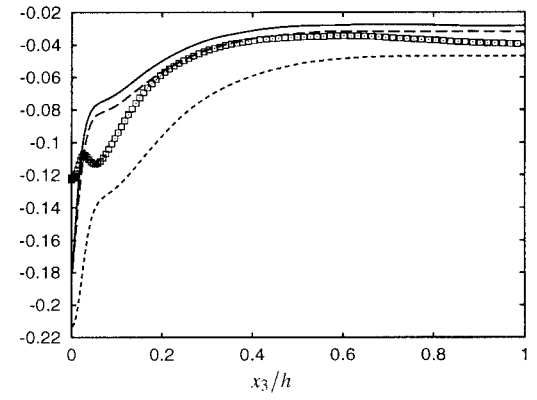

Figure 11: Dissipation of the $\overline{\rho\xi''^2/2}$-balance normalized by χ_w^2/μ_w. ——, $Re_\tau = 545$, $Ma = 3$; – – –, $Re_\tau = 455$, $Ma = 2.5$;- - - -, $Re_\tau = 221$, $Ma = 1.5$. □ shows data of Johansson *et al.*, $Re_\tau = 265$; Sc = 0.7

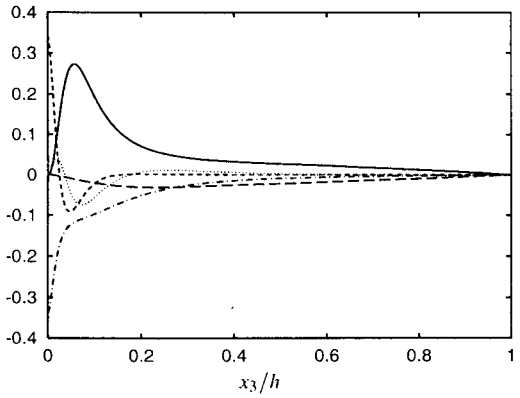

Figure 12: $\overline{\rho u_1'' \xi''}$-balance, $Re_\tau = 545$, $Ma = 3$, normalized by $|\chi_w|\tau_w/\mu_w$. ——, $-\overline{\rho u_1'' u_3''}\frac{\partial \tilde{\xi}}{\partial x_3} - \overline{\rho \xi'' u_3''}\frac{\partial \tilde{u}_1}{\partial x_3}$; – – –, $\overline{\xi''\frac{\partial p}{\partial x_1}}$; - - - -, $\frac{\partial}{\partial x_3}\left(\overline{u_1''\frac{\mu}{Sc}\frac{\partial \xi}{\partial x_3}} + \overline{\xi''\tau_{13}}\right)$; · · · · · · ·, $-\frac{\partial}{\partial x_3}\overline{\rho u_1'' u_3'' \xi''}$; –·–·, $-\overline{\tau_{1j}\frac{\partial \xi''}{\partial x_j}} - \overline{\frac{\mu}{Sc}\frac{\partial \xi}{\partial x_j}\frac{\partial u_1''}{\partial x_j}}$

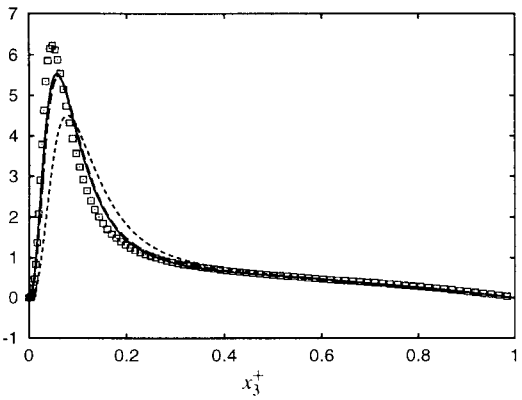

Figure 13: Production of the $\overline{\rho u_1'' \xi''}$-balance, normalized by $u_{av}|\chi_w|/h$. ——, $Re_\tau = 545$, $Ma = 3$; – – –, $Re_\tau = 455$, $Ma = 2.5$;- - - -, $Re_\tau = 221$, $Ma = 1.5$. □ shows data of Johansson *et al.*, $Re_\tau = 265$; Sc = 0.7

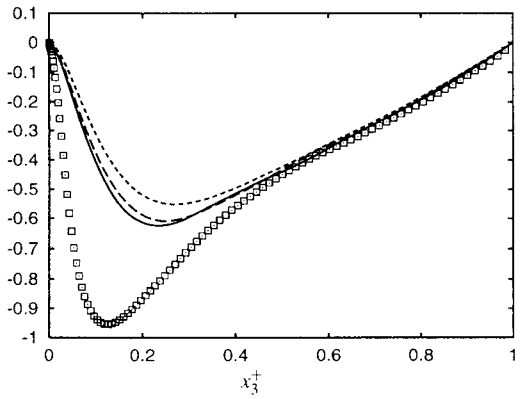

Figure 14: Scalar-pressure-gradient correlation term of the $\overline{\rho u_1'' \xi''}$-balance, normalized by $u_{av}|\chi_w|/h$. ——, $Re_\tau = 545$, $Ma = 3$; – – – , $Re_\tau = 455$, $Ma = 2.5$;- - - -, $Re_\tau = 221$, $Ma = 1.5$. □ shows data of Johansson *et al.*, $Re_\tau = 265$; Sc = 0.7

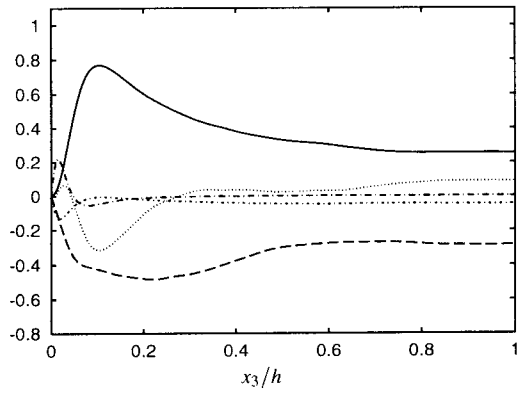

Figure 15: $\overline{\rho u_3'' \xi''}$-balance, Case C, normalized by $u_{av}|\chi_w|/h$. ——, $-\overline{\rho u_3''^2}\frac{\partial \tilde{\xi}}{\partial x_3}$; – – –, $\overline{p\frac{\partial(\xi'')}{\partial x_3}} - \frac{\partial}{\partial x_3}\overline{p\xi''}$; –·–·, $-\frac{\partial}{\partial x_3}\left(\overline{u_3''\frac{\mu}{Sc}\frac{\partial(\xi)}{\partial x_3}} + \overline{\xi''\tau_{33}}\right)$; · · · · · ·, $-\frac{\partial}{\partial x_3}\overline{\rho u_3''^2 \xi''}$; - - - -, $-\overline{\tau_{3j}\frac{\partial \xi''}{\partial x_j}} - \overline{\frac{\mu}{Sc}\frac{\partial \xi}{\partial x_j}\frac{\partial u_3''}{\partial x_j}}$

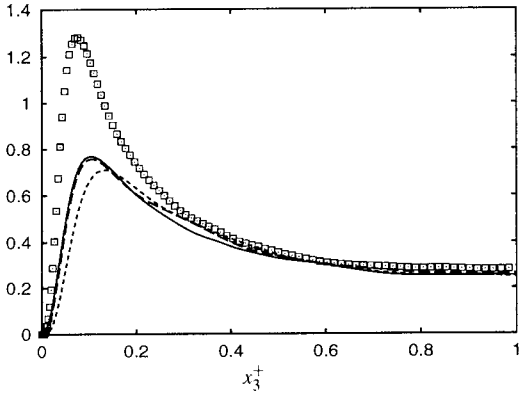

Figure 16: Production of the $\overline{\rho u_3'' \xi''}$-balance, normalized by $u_{av}|\chi_w|/h$. ——, $Re_\tau = 545$, $Ma = 3$; – – –, $Re_\tau = 455$, $Ma = 2.5$;- - - -, $Re_\tau = 221$, $Ma = 1.5$. □ shows data of Johansson *et al.*, $Re_\tau = 265$; Sc = 0.7

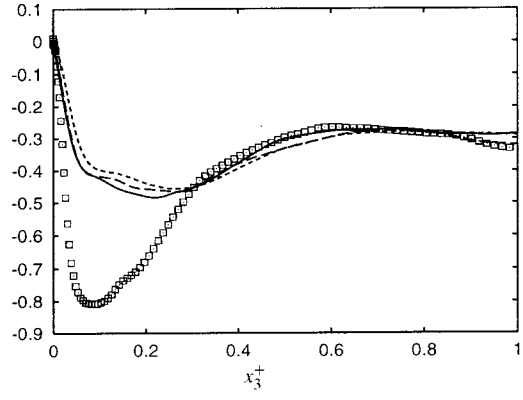

Figure 17: Scalar-pressure-gradient correlation of the $\overline{\rho u_3'' \xi''}$-balance, normalized by $u_{av}|\chi_w|/h$. ——, $Re_\tau = 545$, $Ma = 3$; – – –, $Re_\tau = 455$, $Ma = 2.5$;- - - -, $Re_\tau = 221$, $Ma = 1.5$. □ shows data of Johansson *et al.*, $Re_\tau = 265$; Sc = 0.7